Three-Dimensional Structure and Dynamics of a Brain Specific Growth Inhibitory Factor: Metallothionein-3†

Gülin Öz, Klaus Zangger,‡ and Ian M. Armitage*

Department of Biochemistry, Molecular Biology and Biophysics, University of Minnesota, 6-155 Jackson Hall, 321 Church St. S.E., Minneapolis, Minnesota 55455

Received April 23, 2001; Revised Manuscript Received July 12, 2001

ABSTRACT: The brain specific member of the metallothionein (MT) family of proteins, metallothionein-3, inhibits the growth and survival of neurons, in contrast to the ubiquitous mammalian MT isoforms, MT-1 and MT-2, that are found in most tissues and are thought to function in metal ion homeostasis and detoxification. Solution NMR was utilized to determine the structural and dynamic differences of MT-3 from MT-1 and 2. The high-resolution solution structure of the C-terminal α-domain of recombinant mouse MT-3 revealed a tertiary fold very similar to MT-1 and 2, except for a loop that accommodates an acidic insertion relative to these isoforms. This loop was distinguished from the rest of the domain by dynamics of the backbone on the nano- to picosecond time-scale shown by ^{15}N relaxation studies and was identified as a possible interaction site with other proteins. The N-terminal β-domain contains the region responsible for the growth inhibitory activity, a CPCP tetrapeptide close to the N-terminus. Because of exchange broadening of a large number of the NMR signals from this domain, homology modeling was utilized to calculate models for the β-domain and suggested that while the backbone fold of the MT-3 β-domain is identical to MT-1 and 2, the second proline responsible for the activity, Pro9, may show structural heterogeneity. ^{15}N relaxation analyses implied fast internal motions for the β-domain. On the basis of these observations, we conclude that the growth inhibitory activity exhibited by MT-3 is a result of a combination of local structural differences and global dynamics in the β-domain.

Metallothioneins (MTs)[1] are small (≤ 7 kDa), cysteine-rich proteins that bind both essential (Cu^+, Zn^{2+}) and toxic metals (Cd^{2+}, Hg^{2+}) (*1*). Since their discovery in horse kidney in 1957 (*2*), these proteins have been found in a variety of organisms from animals to higher plants, eukaryotic microorganisms, and some prokaryotes (*3*). Although MTs have been implicated in a variety of functions from metal ion homeostasis and detoxification to oxidative stress response and free-radical scavenging, their primary physiological role remains to be firmly established (*4*). Two extensively studied mammalian isoforms, MT-1 and MT-2, are found predominantly in the liver and kidney but also in many other organs including the brain. In the past decade, two tissue-specific isoforms were discovered, MT-3 in the central nervous system and MT-4 in epithelial cells (*5*, *6*).

MT-3 was discovered during research aimed at understanding the pathogenesis of Alzheimer's disease. Uchida and co-workers established that brain extracts from AD patients stimulated the survival and neurite growth of rat neuronal cultures to a greater degree than normal brain extracts (*7*) due to the loss of a growth inhibitory factor (GIF) (*8*), which was subsequently identified as a member of the metallothionein gene family, MT-3 (*5*). The neurotrophic activity of AD brain extracts and the growth inhibitory activity of MT-3 were confirmed by Erickson et al., but they did not observe a significant decrease of MT-3 or its mRNA in AD brains (*9*).

In addition to the unique growth inhibitory activity of MT-3, several other functional studies have distinguished MT-3 from MT-1 and 2. Transcriptional regulation of MT-3 during development differs from that of MT-1 and 2 (*10*), and MT-3 gene expression does not respond to stimuli such as zinc, cadmium, dexamethasone, and bacterial endotoxin that induce MT-1 and 2 (*11*). One study showed that under zinc deprivation MT-3 competes for the available zinc, unlike MT-1 and 2 that donate their zinc to other zinc requiring proteins and are then degraded (*12*). Therefore, MT-3 likely serves a specific function related to zinc metabolism in the central nervous system rather than being a nonspecific metal

† This work was supported by the NIH Grant DK18778 to I.M.A., the Grant-in-Aid Program of the Office of the Vice President for Research at the University of Minnesota and the Minnesota Medical Foundation Grant MMF/3063-9222-01. G.O. thanks the Graduate School at the University of Minnesota for a Doctoral Dissertation Fellowship. NMR instrumentation was provided with funds from the NSF (BIR-961477), the University of Minnesota Medical School and the Minnesota Medical Foundation Grant MMF: CRF-193-00. The RCSB Protein Data Bank ID for the atomic coordinates of the α-domain of mouse MT-3 is 1JI9.

* Corresponding author. Telephone: (612) 624-5977. Fax: (612) 625-2163. E-mail: armitage@bscl.msi.umn.edu.

‡ Current address: Institute of Chemistry/Organic Chemistry, University of Graz, Heinrichstrasse 28, A-8010 Graz, Austria.

[1] Abbreviations: MT, metallothionein; NMR, nuclear magnetic resonance; AD, Alzheimer's disease; NOESY, nuclear Overhauser effect spectroscopy; TOCSY, total correlation spectroscopy; HMQC, heteronuclear multiple quantum correlation; rmsd, root-mean-square deviation; CV, column volume; LB, Luria broth; CG, circle grow; BHI, brain heart infusion; IPTG, isopropyl-β-D-thiogalactopyranoside; BME, β-mercaptoethanol; DTT, 1,4-dithiothreitol; BHK, baby hamster kidney; SDS, sodium dodecyl sulfate; PAGE, polyacrylamide gel electrophoresis.

10.1021/bi010827l CCC: $20.00
Published on Web 08/29/2001

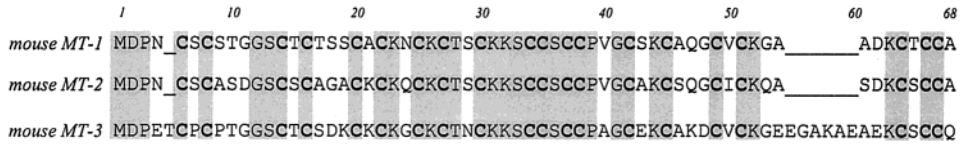

FIGURE 1: Primary sequence comparison of the three metallothionein isoforms in mouse. The conserved cysteines are shown in bold. The residues conserved in all three isoforms are highlighted in gray. The numbering is according to the MT-3 sequence.

distributor. Specifically, MT-3 has been suggested to participate in the utilization of zinc as a neuromodulator since it is expressed in neurons that sequester zinc in their synaptic vesicles (*13*). Another study provided further support for this hypothesis by showing that MT-3 knockout mice are more sensitive to kainate induced seizures than controls since zinc is known to be involved in seizure activity (*14*).

The functional differences between MT-3 and the other mammalian MT isoforms imply structural and/or dynamic differences as well. Three-dimensional structures of mouse MT-1 and several MT-2 isoforms are available (*15*−*19*). These two isoforms have almost identical tertiary structures with the 61−62 amino acid peptide backbone wrapping around two metal clusters in two domains containing three and four divalent metal ions. Using the NMR active isotope of cadmium,$^{113}Cd^{2+}$, it was shown that divalent metals in MTs are tetrahedrally coordinated by bridging and terminal cysteines, 9 in the N-terminal β-domain and 11 in the C-terminal α-domain (*20*). In comparison, MT-3 is a 68-amino acid protein containing two insertions relative to MT-1 and 2: a Thr at position 5 and a glutamate-rich hexapeptide close to the C-terminus (Figure 1). The cysteine residues at conserved positions, lack of histidine and aromatic residues, and the binding of seven divalent metal ions are characteristics common to MT-1, 2, and 3 (*21*). Moreover, electronic absorption, circular dichroism, and one-dimensional ^{113}Cd NMR spectroscopy studies provided evidence that the cluster architecture of MT-3 is similar to MT-1 and 2 (*22*−*25*). The primary sequence of MT-3 is highly homologous to MT-1 and MT-2 (65% sequence identity of mouse MT-3 with mouse MT-1, 56% with mouse MT-2), but MT-3 differs from MT-1 and 2 in its unusual acidity: the overall net charge of apo-human-MT-3 is −3 and apo-mouse-MT-3 is +2 as compared to +4 or +5 for MT-1 and 2. The hexapeptide insertion at the C-terminus is the primary reason for the acidity. Interestingly, another region of MT-3 that is conserved among species, the CPCP tetrapeptide spanning residues 6−9, was shown to be responsible for the growth inhibitory activity. Sewell et al. first showed that the isolated β-domain had a similar level of growth inhibitory activity as the intact protein and then determined that mutating the CPCP sequence to either CTCT or CSCA to resemble MT-1 and MT-2 sequences abolished the inhibitory activity (*21*).

It is of interest to determine what structural and dynamic properties make MT-3 different than MT-1 and 2. Presented in this paper is the first report of the three-dimensional structure of mouse Cd_7-MT-3. Multinuclear/dimensional NMR methods were used to obtain constraints for the structure calculation of the α-domain. Homology modeling was used to calculate models for the β-domain due to its inherent flexibility. Quantitative information about the dynamics of both domains was obtained from heteronuclear NMR relaxation studies using globally ^{15}N labeled MT-3. This structural and dynamic information was compared to information available on MT-1 and MT-2, and the isoform specific characteristics of MT-3 are discussed in relation to its unique growth inhibitory activity and other possible unique functions.

MATERIALS AND METHODS

Mouse Cd_7-MT-3 Expression and Purification. An *Escherichia coli* strain BL21(pLysS) that contained the expression vector pET3d (Novagen) encoding mouse MT-3 was kindly provided by Dr. Dennis R. Winge at University of Utah. The plasmid was retransformed into the *E. coli* strain BLR(DE3). LB starter cultures (5 mL) were inoculated with 5 μL of glycerol stock and grown for 4−6 h before they were used to inoculate 200-mL LB cultures with 5%(v/v) preculture. After 3 h, the 200-mL cultures were pelleted, resuspended in BHI media, and used for inoculation of fresh CG medium with 1.5% (v/v) preculture. All cultures were grown at 37 °C with 150 mg/L ampicillin. Expression of MT-3 was induced with 1 mM IPTG at an OD_{600} of 1.2, followed by a 30-min growth before addition of 0.4 mM $CdSO_4$. Cells were harvested 12 h post-induction, pelleted, washed with 20 mM Tris-HCl, 0.25 M sucrose, pH 8.0, and resuspended in the same buffer with 0.04% BME. They were lysed with a French pressure cell (SLM Aminco) and centrifuged to remove cell debris. The supernatant was loaded onto a POROS HQ 20 (PerSeptive Biosystems) anion exchange column (2 × 25 cm) equilibrated with 20 mM Tris-HCl, pH 7.6, and run with an Äkta FPLC system (Amersham Pharmacia Biotech). After column was washed with 3.5 CV of the same buffer, MT-3 was eluted with 85 mM NaCl. Elution was monitored at 280, 254, and 220 nm, and the cadmium content of the fractions was assessed by atomic absorption spectroscopy (Varian SpectrAA-100). The first column produced 70% pure MT-3 which was treated with 10 mM DTT overnight before impurities were precipitated with 2 M ammonium sulfate. To bind the remaining impurities, the supernatant was passed over an Octyl Sepharose (Amersham Pharmacia Biotech) column (2.6 × 3 cm) equilibrated with 2 M $(NH_4)_2SO_4$ (*9*). The flow-through contained pure MT-3 based on SDS−PAGE but also higher molecular weight aggregates that needed to be separated by a final gel filtration step. The sample was dialyzed against 20 mM Tris-HCl, pH 7.6, concentrated by ultrafiltration (Amicon, YM3 membrane) in the presence of 7.5 mM DTT and run over a Sephadex G-75 (Sigma) gel filtration column (2.6 × 80 cm) equilibrated with 20 mM Tris-HCl, pH 7.6.

Metal-to-protein ratios were determined by measuring the metal content by atomic absorption spectroscopy, the sulfhydryl content by the colorimetric 5,5′-dithiobis(nitrobenzoic acid) (DTNB) reaction in 6 M guanidine hydrochloride (*26*) and by assuming that each molecule of MT-3 contained 20 thiolates. Electronic absorbance measurements were performed with a Beckman DU 7400 diode array UV−visible

spectrophotometer. The protein concentration was also confirmed by total amino acid analysis.

Replacement of natural abundance cadmium with the NMR-active $^{113}Cd^{2+}$ was accomplished as described previously (*27*). Briefly, the sample was treated with 40-fold excess DTT and its pH lowered to approximately 1.5 to remove the metals. The sample was then desalted with a Sephadex G-25 (Sigma) gel filtration column (1.6 × 26 cm) equilibrated with 25 mM HCl. After determination of the apo-MT-3 concentration in the protein containing pool by the DTNB reaction, 8 equivalents of $^{113}Cd^{2+}$ were added and the sample was kept under argon for 20 min. The pH was quickly increased to 7−8 with 200 mM Tris base and the sample was treated with Chelex-100 to remove excess metals.

To prepare samples for NMR, the Tris buffer was exchanged with either 15 mM potassium phosphate or 20 mM Tris-HCl-*d* (Tris-d_{11} from Isotec Inc.) by washing the concentrated samples in a model 8MC Micro-Ultrafiltration system (Amicon) several times. All NMR samples contained 10% D_2O and 0.02% sodium azide.

Global ^{15}N Labeling of Mouse Cd_7-MT-3. The *E. coli* strain BLR(DE3) was not suitable for growth in minimal media. Therefore, the plasmid encoding MT-3 was retransformed into the BL21(pLysS) strain for ^{15}N labeling of the protein. LB starter cultures grown overnight were used to inoculate M10 minimal media (*28*), that contains 1 g/L $(^{15}NH_4)_2SO_4$ (Isotec Inc.), with 0.5% preculture. Following IPTG induction at OD_{600} 1.2 and addition of $CdSO_4$, cultures were grown overnight at 37 °C in the presence of 150 mg/L ampicillin before harvesting. The above purification protocol yielded 3 mg of labeled protein/L of culture grown.

NMR Spectroscopy. Two-dimensional homonuclear NOESY (*29*) and TOCSY (*30*) spectra were acquired using an 800 MHz Varian Unity INOVA spectrometer in the phase-sensitive mode with the States-Haberkorn method (*31*) with mixing times of 50, 100, and 150 ms for NOESY and 30 and 60 ms for TOCSY experiments. Solvent suppression was accomplished using the WATERGATE sequence (*32*). To resolve resonance overlap, spectra were acquired at 10, 20, 30, 40, and 50 °C. The ^1H chemical shifts were referenced to the residual water signal (4.76 ppm at 25 °C) after correcting for temperature (*33*). All spectra were recorded with 256 t_1 increments each containing 64 transients of 1024 complex data points. Prior to Fourier transformation, the data sets were zero-filled in F_1 dimension to 1024 complex points and multiplied by a 60° shifted squared cosine window function in both dimensions. The TOCSY pulse sequence contained a DIPSI-2 (*34*) spin-lock field at 13 kHz.

^1H-^{113}Cd HMQC spectra (*35*) were acquired with a 600 MHz Varian Unity INOVA spectrometer at 30 °C. The external standard 0.1 M $Cd(ClO_4)_2$ was used for referencing the ^{113}Cd signals. The solvent signal was suppressed by presaturation. ^1H-^{113}Cd coupling constants in metallothioneins vary between 5 and 60 Hz; therefore, preparation delays $1/2J^{H-Cd}$ were varied accordingly and spectra acquired for coupling constants of 10, 20, 30, 40, 50, and 60 Hz. Cd decoupling was performed during acquisition using a WALTZ-16 sequence (*36*). A spectral width of 16 000 Hz was observed in the Cd dimension, and 64 transients of 1024 complex data points were acquired for each of the 128 t_1 increments. The data sets were processed the same way as the homonuclear experiments.

Additional cadmium-to-cysteine connectivities were obtained from 1D ^1H NMR experiments with selective gated decoupling of specific Cd resonances. The difference spectra contained resonances only from the cysteines coordinating the selected cadmium.

The ^{15}N relaxation data was acquired with a 3 mM globally ^{15}N labeled mouse MT-3 sample in 20 mM Tris-HCl-*d*, pH 6.5, at 10 °C on a 600 MHz Varian Unity INOVA spectrometer. Standard pulse sequences for T_1, T_2, $T_{1\rho}$ and heteronuclear NOE (*37*) were used with 160 t_1 increments, 16 transients, and 1024 complex data points. τ_{CPMG} in the T_2 experiments was 1.17 ms. The $T_{1\rho}$ experiments were performed with a spin lock field of 1.35 kHz. The heteronuclear NOE experiment contained a 3.5 s proton presaturation period whereas the NONOE experiment employed a relaxation delay of 3.5 s. T_1 values were determined from spectra with relaxation delays of 10, 50, 100, 200, 300, 450, 600, 850 ms, and T_2 and $T_{1\rho}$ values were determined from spectra with relaxation delays of 10, 30, 50, 70, 90, 110, 130, and 170 ms by fitting the peak intensities to a single-exponential decay function with the program NMRView (*38*). The steady-state NOE values were determined from the ratio of peak intensities in the NOE and NONOE spectra. The errors were determined by double recording the 200 ms experiment for T_1 and the 70 ms experiment for T_2 and $T_{1\rho}$. The errors in the NOE and NONOE experiments were determined from the baseline noise in the spectra. ^{15}N chemical shift assignments were accomplished with 3D TOCSY−HSQC and NOESY−HSQC experiments. To determine the overall rotational correlation time, τ_m, the residues whose T_1/T_2 values were within one standard deviation from the average were used (*39*).

The ^1H and ^{15}N chemical shifts of the α-domain at 10 °C have been deposited in BioMagResBank (BMRB accession number: 5066).

Structure Calculations. The structure of the α-domain which consists of the amino acid residues Lys32−Gln68 was calculated using X-PLOR 3.851 (*40*) on an SGI IRIS Indigo Impact 10000 computer. The cadmium−sulfur cluster was defined in X-PLOR as two patch residues, and the structure calculations were done as described previously (*19*) using the hybrid distance geometry-dynamical simulated annealing protocol (*41*). Briefly, the calculation consisted of the generation of 50 substructures from a covalent starting structure by the distance geometry approach using the NOE constraints followed by two consecutive Powell minimization and simulated annealing protocols for the refinement of these structures. The strong, medium, and weak NOE constraints had upper and lower distance limits of 1.8−2.7, 1.8−3.3, and 1.8−5 Å, respectively. The upper distance limit was increased by 0.5 Å for NOEs that involved pseudoatom methyl and methylene groups. Structures with one or no NOE violations (greater than 0.5 Å deviation from the NOE), an rmsd for deviations from ideality of less than 0.01 Å for bonds and less than 5° for angles were selected as final structures, and 10 of these with the lowest energies were used to calculate the average. These 10 models were evaluated with the program PROCHECK (*42*). A total of 58.1% of the residues were found in the most favored regions of the Ramachandran plot, 35.5% in additional allowed regions, 6.5% in generously allowed regions, and none in disallowed regions. The average structure was minimized

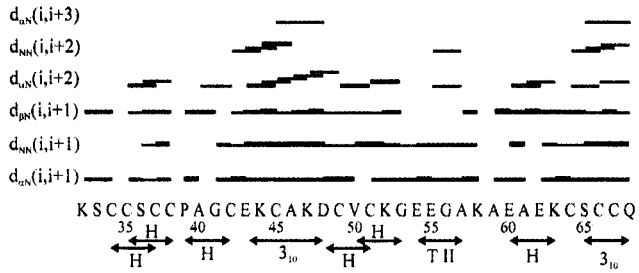

FIGURE 2: Summary of sequential and medium range NOEs in the α-domain of mouse MT-3. Thickness of the lines corresponds to the NOE intensity. Secondary structural elements are indicated below the sequence with 3_{10} for the 3_{10}-helices, H for half-turns, and T II for the type II turn.

using the same protocol as for structure refinement. Superposition of structures and rmsd calculations were done with InsightII 97.0 (Biosym/MSI).

Homology Modeling. The program MODELLER-4 was used for multiple sequence alignment homology modeling (*43*). The cadmium ions were included as "block" residues that are restrained to the conformation of the equivalent atoms in the templates. Models were calculated both with and without inclusion of the metal cluster constraints (cadmium−sulfur bond length, Cd−S−Cd, S−Cd−S, and CysC^{β}−S−Cd bond angles (*19*)), and the two methods resulted in identical structures. The 10 lowest energy models out of 50 calculated models were evaluated with PROCHECK (*42*). A total of 60.9% of the residues were in the most favored regions of the Ramachandran plot, 34.8% were in additional allowed regions, and 4.3% in disallowed regions. These values are comparable to the quality of the published MT structures.

RESULTS

Protein Expression and Purification. MT-3 has typically been expressed in the *E. coli* strain of BL21(pLysS), but considerable overexpression of the protein has not been observed using this protocol as judged by the lack of a strong induced protein band on Coomassie-stained SDS−polyacrylamide gels (*25*). Retransforming the plasmid into the BLR-(DE3) strain and using a different growth protocol as explained in the materials and methods section resulted in Cd_7-MT-3 being 25% of the total soluble protein determined by SDS−PAGE of whole cell extracts (data not shown). The yields of 15 mg/L of culture after the first column in the purification protocol and 8−9 mg/L by the end of the purification provided the quantities of protein required for NMR studies.

Sequential Resonance Assignments, Secondary Structural Analysis and Metal Cluster Structure of the C-Terminal α-Domain. The solution structures of the two domains of all MTs studied by NMR have been calculated separately due to a lack of interdomain connectivities (*15*−*19*). Therefore, the domains of MT-3 were also investigated separately. The ^{1}H NMR sequential assignments were accomplished using the standard protocols described in the literature with TOCSY experiments for spin system assignments and NOESY experiments for sequential assignments (*44*).

Figure 2 shows a summary of the sequential and medium-range NOEs of the α-domain of mouse MT-3. The observed

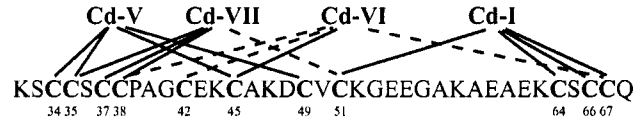

FIGURE 3: Cd-to-Cys connectivities in the α-domain of mouse MT-3 extracted from the ^{1}H-^{113}Cd HMQC spectra and 1D ^{1}H experiments where selective ^{113}Cd decoupling was used. The connectivities shown with broken lines are to the cysteines selected from two or three cysteines with degenerate chemical shifts after calculating all possible structures. The cadmium ions are labeled according to decreasing frequency.

secondary structural elements are two 3_{10} helices, several half-turns, and a type II turn. Even though the primary sequence of the hexapeptide insertion (Glu55−Glu60) suggests a propensity for helical structure (*45*, *46*), our NMR data did not contain the NOE signatures of an α-helix for these residues. In fact, this region was the least well-defined portion of the α-domain (see below).

Since MT-3 did not contain many regular secondary structural elements and as a result did not produce as many medium and long range NOEs as normally required for a high precision 3D structure determination, establishment of the cysteine-β-proton-to-metal connectivities was important. These connectivities were obtained from ^{1}H-^{113}Cd HMQC spectra and 1D ^{1}H NMR experiments where selective Cd decoupling was used.

The ^{113}Cd chemical shifts are very sensitive to chemical environment (for review see ref *47*). All of the ^{113}Cd resonances of mouse MT-3 were in the same chemical shift range as MT-1 and 2, indicating that the Cd^{2+} ions in MT-3 are tetrahedrally coordinated by cysteines in similar cluster structures as MT-1 and 2. This was verified by HMQC experiments for Cd-I and Cd-V which were found to be coordinated by the same cysteines as in MT-1 and 2 (Figure 3). Proton chemical shift degeneracy prevented unambiguous assignment of all four coordinating cysteines of Cd-VI and Cd-VII. The connectivities that were established with certainty are shown with solid lines in Figure 3 and were identical to MT-1 and 2 connectivities. To overcome the ambiguity problem, 10 structures were calculated for all possible combinations of Cd-VI and Cd-VII coordinations. All combinations other than the typical MT-1 and 2 cluster arrangement resulted in distorted coordination geometries around the cadmiums and/or in structures with high energy. Therefore, we conclude that the α-domain cluster structures of MT-1, 2, and 3 are the same. All connectivities were used for further structure calculations.

Structure of the α-Domain. A total of 377 NOEs, 47 of which were long range (d_{ij}, $j > i + 4$), and the 16 Cd-to-Cys connectivities were used for the structure calculation (Figure 4). The backbone conformation of MT-3 shows striking similarity to MT-1 and MT-2 despite the acidic hexapeptide insertion. A superposition of the minimized average structures of mouse MT-3 and mouse MT-1 over the backbone atoms of the first 20 residues of the α-domain, i.e., the region preceding the insertion, resulted in an rmsd for the backbone atoms of only 1.52 Å (Figure 5). The main difference between the MT-1 and MT-3 structures lies in the loop between residues Lys52 and Glu60, where the acidic insertion is located. Inspection of Figure 4 shows a lack of long-range NOEs and an overall low number of NOEs throughout this region which resulted in disorder in the

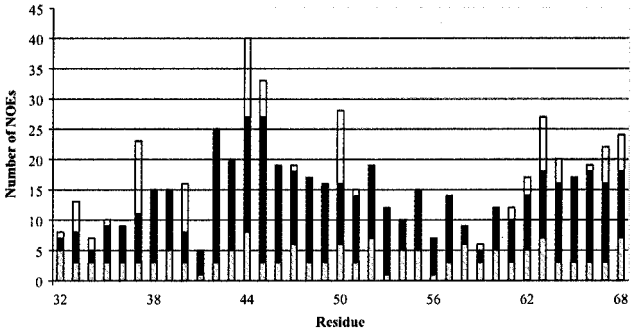

FIGURE 4: Number of NOE constraints plotted as a function of residue number in the mouse MT-3 sequence. Long-range NOEs (d_{ij}, $j > i + 4$) are shown in white, short and medium range NOEs are shown in black, and intraresidue NOEs are shown with crosshatched bars.

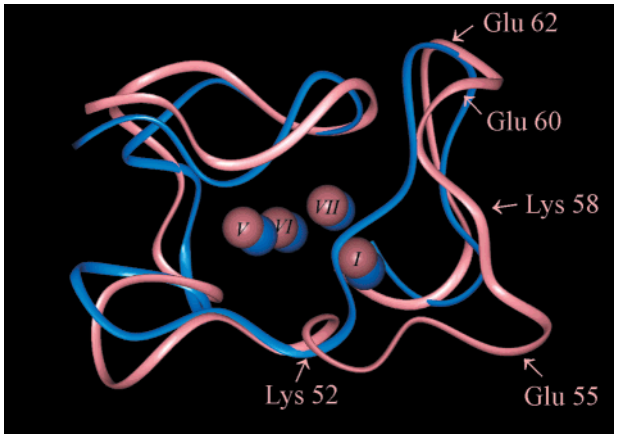

FIGURE 5: Superposition of the minimized average structures of the α-domain backbones of mouse MT-1 (blue) and mouse MT-3 (pink). Some residues on the insertion loop are labeled for easier orientation. The cadmium ions are shown as spheres and labeled according to decreasing frequency.

Table 1: Structural Statistics of the α-domain of Mouse MT-3[a]

	⟨SA⟩	⟨SA⟩$_{av}$
Energies[b] (kcal/mol)		
$E_{overall}$	439.54 ± 10.66	413.18
E_{bonds}	31.539 ± 1.05	30.943
E_{angles}	192.6 ± 8.20	178.5
E_{vdW}	29.03 ± 3.28	25.22
rms Deviations from Covalent Geometry used within X-PLOR		
bonds (Å)	0.00786 ± 0.00013	0.00779
angles (deg)	1.923 ± 0.074	1.740
impropers (deg)	0.7162 ± 0.0571	0.7244
NOEs (Å)	0.0944 ± 0.0024	0.0921
Atomic rms Differences ⟨SA⟩ vs ⟨SA⟩$_{av}$		
all non-hydrogen atoms (Å)	1.144	
backbone atoms (Å)	0.707	

[a] The statistics refer to the 10 lowest energy NMR structures and the energy-minimized average structure. The structures were superimposed over the backbone atoms. [b] Energies were calculated using a square well potential term for NOE terms (100 kcal mol^{-1} Å^{-2}) and a square well quadratic energy function for the torsional potential (500 kcal mol^{-1} rad^{-1}). The force constant for covalent bonds was 1000 kcal mol^{-1} Å^{-2}.

calculated models (Figure 6). An rmsd for the backbone atoms of the 10 best structures was 0.37 Å when residues Ser33−Lys52 and Glu60−Gln68 were superimposed, whereas it was 0.7 Å for the whole α-domain (Table 1).

Table 2: Results of the Modelfree Analysis of the ^{15}N Relaxation Data for the α-Domain of Mouse MT-3

model[a]	residues best described by the model
1 (S^2)	C35, S36, C38, A40, G41, E43, A46, K47, C49, V50, S65, C66
2 (S^2, τ_e)	C42, K44, C45, K52−C64, C67, Q68
3 (S^2, R_{ex})	C51
4 (S^2, τ_e, R_{ex})	D48

[a] See text for description of parameters.

Dynamics of the α-Domain. A static picture only partially explains the biochemical characteristics of a protein. Additionally, in the case of MT-3, it was necessary to address the question as to whether the disorder observed for the acidic loop was static or dynamic. Therefore, ^{15}N relaxation studies were performed. Nitrogen-15 T_1, T_2, $T_{1\rho}$ and the steady-state {^{1}H}-^{15}N NOE values for the backbone amide groups were measured using globally ^{15}N labeled mouse MT-3. As seen in Figure 7, ^{15}N T_1 values were rather homogeneous over the α-domain except for Asp48 and the C-terminal residue Gln68 with an average of 603 ± 62 ms. The average T_2 was 113 ± 23 ms. Increased T_2 values were observed for residues Asp48, Lys52−Ala61, and Gln68. The same residues also displayed low NOEs (< 0.6). The increased T_2 and low NOE values are indicative of internal dynamics on the pico- to nanosecond time scale and therefore prove that the disorder observed for the acidic loop is dynamic in character.

A ratio of the rotating frame relaxation time, $T_{1\rho}$, to the transverse relaxation time, T_2, greater than 1 is indicative of chemical/conformational exchange on the micro- to millisecond time scale. This ratio averaged 1.01 ± 0.05 for the α-domain without significant deviations along the sequence, and hence there was no evidence for exchange on this time scale.

To present a clearer picture about the types of motion the backbone of each residue displays, the extended model-free spectral density function was fit to the relaxation data with the program Modelfree 4.01 (*48*), which is based on the formalism developed by Lipari & Szabo (*49*, *50*). Using this program and a statistical approach, one set of model-free parameters was selected for each residue that best describes its relaxation data. The results are summarized in Table 2. The model that only includes the order parameter, S^2, indicates relative rigidity and lack of extensive internal dynamics. The next model includes S^2 and an effective internal correlation time, τ_e, for motions faster than the overall rotational correlation time, τ_m, that was found to be 7.03 ns. The residues that span the acidic insert, Glu55−Glu60, are in the group that was best fit by this second model and therefore exhibit motions on a time scale faster than 7.03 ns. The parameter R_{ex} describes an exchange contribution on the micro- to millisecond time scale, and Asp48 and Cys51 were the only residues that showed dynamics on this time scale. This result is in agreement with the $T_{1\rho}$-to-T_2 ratios of 1 mentioned above. Two residues, Cys34 and Cys37, were not fit by any of the models, indicating more complex dynamics for these residues.

Structure of the β-Domain. Most of the expected spin systems of the β-domain were identified in the aliphatic region of the TOCSY spectra. The fingerprint region of the NOESY spectra, on the other hand, did not contain all the cross-peaks necessary for the complete sequential assignment

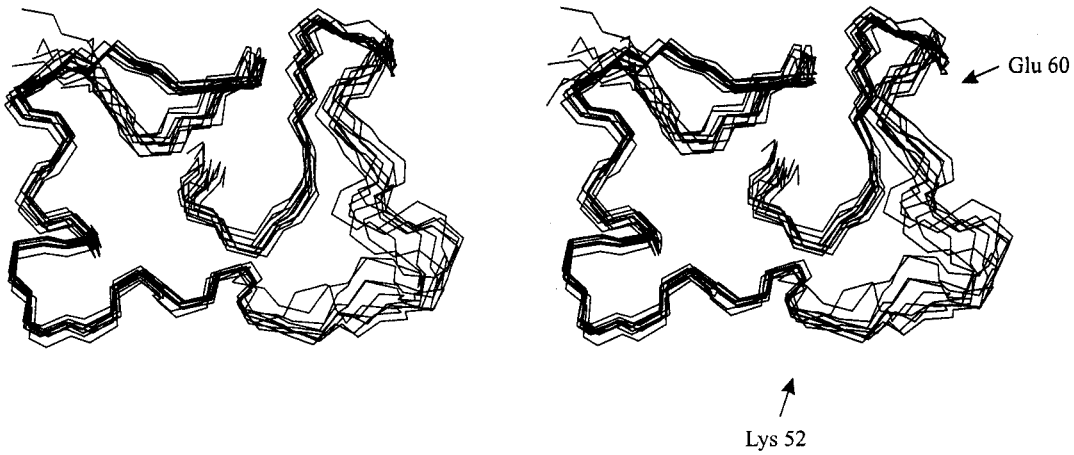

FIGURE 6: Stereoview of the superposition of the 10 lowest energy structures of Cd_7-MT-3 α-domain. The figure was prepared with the program MOLMOL (*67*) in divergent view. The N-terminus points outward, the C-terminus points inward.

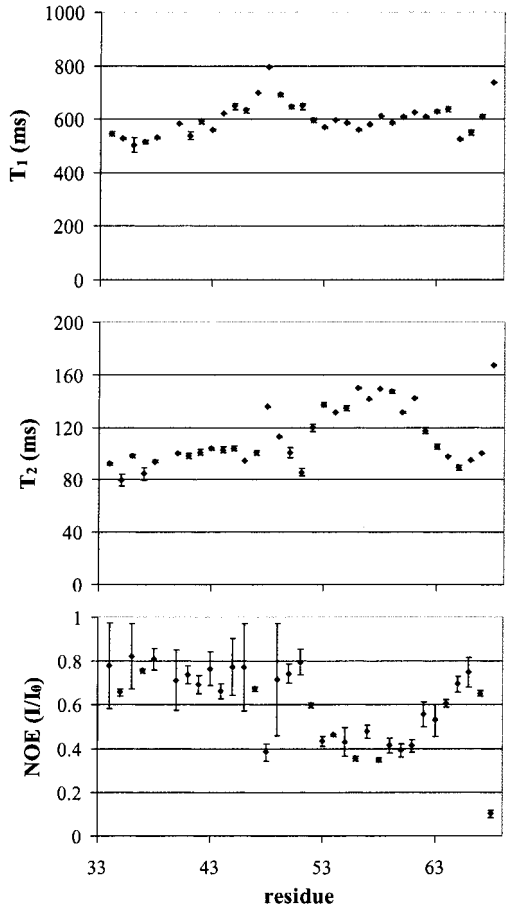

FIGURE 7: ^{15}N backbone amide relaxation parameters of the α-domain of Cd_7-MT-3 as a function of residue number.

of this domain. This was most likely due to conformational exchange broadening, and a number of different solution conditions and the temperature range studied (10−50 °C) did not overcome the problem. To slow the exchange processes, NMR data was also acquired at −10 °C in the presence of deuterated methanol which resulted in almost complete loss of resolution due to increased viscosity. Surprisingly, the only portion of the domain that permitted sequential assignments was the first seven residues that partly contain the $C_6P_7C_8P_9$ tetrapeptide to which the growth inhibitory activity has been mapped (*21*). The ^1H-^{113}Cd HMQC spectra also contained very few cross-peaks from the β-domain. Interestingly, in the presence of 40 molar equivalents of deuterated-DTT, the ^1H-^{15}N HSQC spectrum of a 3 mM, globally ^{15}N labeled MT-3 sample contained additional cross-peaks that were assigned to the β-domain. Several of these new resonances were sequentially assigned by 3D TOCSY−HSQC and NOESY−HSQC experiments, increasing the fraction of the β-domain that was sequentially assigned to about half of the domain. However, no new structural constraints were obtained from these spectra. Since DTT itself has affinity for metals (*51*), the observed effect could be due to metal removal from the β-domain by DTT and unfolding of the domain as a consequence. This possibility was ruled out by determination of the metal and protein concentrations by atomic absorption spectroscopy and amino acid analysis, respectively, before and after dialysis of the sample whereby DTT was removed. Determination of translational diffusion coefficients by pulsed-field gradient NMR suggested stabilization of the β-domain by self-association as the reason of the new resonances in the presence of DTT.

Since the structure of the β-domain could not be experimentally derived by NMR, we used homology modeling to calculate models for this domain based on the published structures of the other mammalian MT isoforms. Mouse MT-1 (*19*), human MT-2 (*17*), rabbit MT-2 (*15*), and rat MT-2 (*16*), that have 68, 65, 61, and 65% identical β-domain sequences, respectively, were used as templates. Fifty models were calculated with the program MODELLER-4 (*43*). It was established that the few NOEs obtained for the β-domain were not violated in these models. The models had superimposable backbone folds to the MT-1 and MT-2 structures. Therefore, the primary sequence of the MT-3 β-domain can be accommodated in a similar structure as the other mammalian isoforms even though this may not be the only conformation adopted by the β-domain in solution (see Discussion). Interestingly, the side chain of Pro9, one of the two prolines responsible for the growth inhibitory activity, was found in two conformations in the calculated models (Figure 8). Both of these conformations were in the trans conformer of the Xxx−Pro bond. We observed more proline cross-peak patterns than expected in the aliphatic region of the TOCSY spectra, and this observation might well be a consequence of two possible conformations of Pro9.

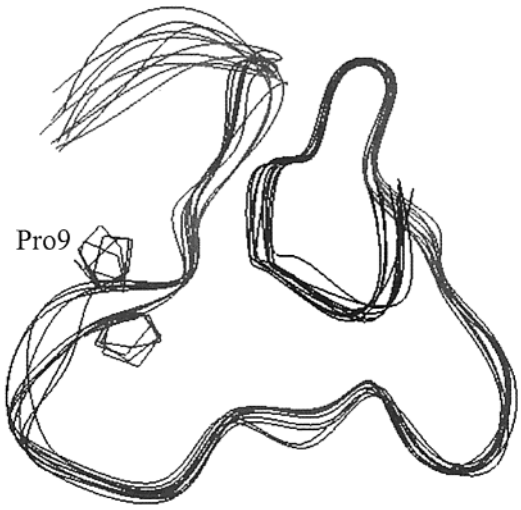

FIGURE 8: Superposition of the 10 lowest energy models of Cd_7-MT-3 β-domain calculated with MODELLER-4. The side chain of Pro9 is shown. The figure was prepared with the program InsightII 97.0.

Dynamics of the β-Domain. The absence of most of the connectivities involving the amide resonances from the β-domain in the homonuclear correlation spectra implied disorder in this domain. Nitrogen-15 relaxation data was analyzed for a more quantitative evaluation of this disorder. Cross-peaks in the ^{15}N-^{1}H HSQC spectra that could not be sequentially assigned but were also not assigned to the α-domain were assigned to the β-domain and the backbone amide ^{15}N relaxation parameters were investigated for these cross-peaks. An average T_1 of 578 ± 61 ms and an average T_2 of 133 ± 59 ms were observed for these 18 residues. The NOE data were unreliable in this case due to the low intensities of these cross-peaks and inherent insensitivity of the NOE experiments. Nevertheless, the shorter T_1 and longer T_2 values indicate increased internal dynamics on the nanosecond to picosecond time scale in this domain as compared to the α-domain. The $T_{1\rho}$-to-T_2 ratios of these resonances that were detectable did not deviate significantly from 1 either as observed for the α-domain indicating the absence of exchange processes on a micro- to millisecond time scale.

DISCUSSION

The α-Domain. In the mammalian MT-1 and MT-2 structures reported thus far, there are no α-helices or β-sheets, but two stretches of 3_{10} helices between residues 42−47 and 57−61 (based on the mouse MT-1 sequence) and several type II turns and half-turns (*16*, *17*, *19*, *52*). These secondary structural elements and the overall fold of the α-domain were found to be conserved in MT-3 with some additional turns relative to MT-1 and 2.

The main difference in the structure of the α-domain of MT-3 was the loop that spans residues Lys52−Glu60 and contains the acidic hexapeptide insertion. The ^{15}N relaxation analysis showed that this loop exhibits rapid internal motions. Many unstructured and flexible regions in proteins have been recognized to be involved in important regulatory functions in the cell, such as cell cycle control and transcriptional and translational regulation (*53*). In most cases, these unstructured regions have been shown to assume structure upon binding a target molecule. No physiological significance has yet been assigned to the acidic insertion in MT-3, but it has been suggested that this protein interacts with other proteins in vivo (*9*, *24*). Therefore, this loop might be forming an acidic surface for such an interaction. Considering this possibility, one may speculate that binding of a factor might favor one conformation over the others, for example, an α-helix as predicted based on primary sequence analyses (*45*, *46*). The acidic insertion and the possible functionality that it may provide to MT-3 is also interesting in light of the recent suggestion that proteins with very similar sequences can gain additional functional sites during evolution (*54*). Thus, MT-3 shares its overall fold and metal binding properties with MT-1 and 2, yet accommodates a possible additional interaction site with other molecules.

The β-Domain. The $C_6P_7C_8P_9$ tetrapeptide of the β-domain of MT-3 has attracted most of the attention with regard to the growth inhibitory activity. The first structural information obtained in this study about this region was that two conformations of Pro9 can be accommodated in the MT-3 structure. A recent study has shown that both prolines are necessary for the biological activity (*55*), and the general consensus is that they function in a protein−protein interaction since proline-rich regions are known to mediate such interactions (*56*). Thus, our observation suggests specific roles for these two prolines in such an interaction.

Recently, it was suggested that the Cys−Pro bonds in the $C_6P_7C_8P_9$ tetrapeptide undergo a slow cis/trans isomerization accompanying partial unfolding of the β-domain based on the broad and low intensity ^{113}Cd resonances from the β-domain of human MT-3 (*55*). Although the 1D ^{113}Cd and 2D ^{1}H-^{113}Cd HMQC spectra of mouse MT-3 were in agreement with this previous observation, our 2D NOESY spectra did not show any evidence for the *cis*-conformation of any of the Xxx-Pro bonds.

Another structural difference of the β-domain was revealed by NMR sequential assignments. The fact that the first seven residues (13 in the presence of DTT) were the only sequentially assigned part of this domain was in stark contrast to previous experience with MT-1 and 2, where the structure of the N-terminal 12 residues was less well defined than the rest of the domain (*15*−*17*, *19*). The conformational flexibility of this region in MT-3 is most likely restricted by the prolines, while the resonances from the rest of the domain get broadened beyond detection due to conformational exchange. Conformational exchange, that did not cause broadening as severe as in the present case, was indicated for the β-domain of sea urchin MTA by ^{15}N relaxation studies (*57*). Unfortunately, no mammalian MTs other than MT-3 have been studied by ^{15}N relaxation so far. The relaxation analysis of the detectable β-domain resonances from MT-3 showed no indication of exchange on the micro- to millisecond time scale. However, this method is sensitive to exchange processes slower than the spin-lock field used in the $T_{1\rho}$ experiment (1.35 kHz) and faster than the effective spin-lock field used in the T_2 experiment ($1/(2\tau_{CPMG}) = 427$ Hz). Therefore, it is possible that exchange outside these boundaries was not detected.

The average ^{15}N T_1 and T_2 data from the β-domain did, however, indicate nano-to-picosecond time scale motions. This analysis assumes that the α- and β-domains exhibit the same overall rotational correlation times. It is possible that

the domains move independently with different correlation times due to their size difference. One can calculate the expected rotational correlation times for the isolated domains using an empirical equation (*58*). This calculation resulted in an expected rotational correlation time of 4 ns for the 31 residue β-domain and 4.75 ns for the 37 residue α-domain. The percentage difference between these numbers correlates with the observed difference in T_1 and T_2 values of the two domains. However, previous studies with proteins containing two dynamically independent domains have shown that the actual differences in correlation times of the domains are much less than expected based on size difference because the presence of one domain affects the correlation time of the other even though the motions of the two domains are not correlated (*59*). Therefore, we conclude that the different T_1 and T_2 values of the β-domain are a consequence of internal dynamics rather than a shorter rotational correlation time of this domain as compared to the α-domain.

To better understand the reason for the conformational flexibility of the β-domain, we turned to primary sequence analysis. An abundance of serines, prolines, and charged residues has been associated with protein disorder (*60*). Specifically, the so-called PEST sequences, sequences rich in proline, glutamic acid, serine, and threonine, exhibit conformational flexibility and target proteins for degradation by the proteasome complex (*61*, *62*). The N-terminal 19−21 residues of MT-3, i.e., 2/3 of the β-domain, were identified as a possible PEST sequence, whereas MT-1 and MT-2 were not found to contain likely PEST sequences (*63*). Whether or not part of the MT-3 β-domain acts as a PEST sequence in vivo and targets the protein to degradative pathways remains to be established experimentally. Nevertheless, it is tempting to speculate that this may provide a mode of regulation of MT-3 turnover that is different from MT-1 and MT-2 which are thought to be degraded in lysosomes (*64*). More importantly, this finding reveals the fact that the amino acid composition of MT-3 meets the criteria for flexible protein regions despite the apparent sequence homology to MT-1 and 2.

In light of the new dynamics information about the β-domain of MT-3, a pattern becomes apparent among the family of mammalian metallothioneins. In all the mammalian MT structures characterized to date, the β-domains were found to be less well defined and more flexible than the α-domains (*15*−*17*, *19*). Zangger et al. compared the ratios of the NOEs obtained from the β- and the α-domains between MT-1 and MT-2s and showed that the β-domain of MT-1 is considerably less well defined than in MT-2 (*19*). We found this ratio to be even smaller in the case of MT-3: While the 377 NOEs made the structure of the α-domain the best defined mammalian MT domain to date with more than 16 NOEs per residue, the β-domain did not even exhibit sufficient cross-peaks for complete sequential assignments. On the basis of these results, we suggest that the dynamics of the β-domains of mammalian metallothioneins has been fine-tuned for their specific functions. Even though no functional differences between MT-1 and MT-2 isoforms have been revealed to date, their reported differential expression (*65*, *66*) and the mere existence of different isoforms argues for a difference in functional properties of these isoforms, too.

In summary, the present work showed that (i) the acidic hexapeptide insertion in MT-3 has been incorporated into the α-domain in a flexible loop such that the domain has the same metal cluster and a very similar tertiary fold compared to MT-1 and 2, (ii) the β-domain exhibits more rapid internal dynamics as compared to MT-1 and 2, which likely is related to the specific function of MT-3, and (iii) in contrast to MT-1 and 2, the first 13 residues of the β-domain of MT-3 have a more rigid conformation than the rest of the domain and Pro9 can assume one of two conformations suggesting local structural differences to be another reason for the activity differences between MT-3 and the other mammalian MT isoforms.

ACKNOWLEDGMENT

The authors would like to thank Ms. Carmen Silvers for technical assistance, Ms. Melissa McCornack and Dr. Ryan McKay for helpful suggestions on the manuscript, Drs. David H. Live and Beverly Gaul Ostrowski at the Structural Biology High Field Nuclear Magnetic Resonance Facility of the University of Minnesota for assistance with the NMR instrumentation, Dr. Andras Fiser for assistance with MODELLER-4, and Dr. David A. Okar for invaluable discussions and suggestions. NMR data analysis and structure calculations were done at the Basic Sciences Computing Laboratory of the Supercomputing Institute at the University of Minnesota.

REFERENCES

1. Kägi, J. H. R., and Schäffer, A. (1988) *Biochemistry 27*, 8509−8515.
2. Margoshes, M., and Vallee, B. L. (1957) *J. Am. Chem. Soc. 79*, 4813−4814.
3. Binz, P., and Kägi, J. (1999) in *Metallothionein IV* (Klaassen, C. D., Ed.) pp 7−13, Birkhäuser Verlag, Basel.
4. Palmiter, R. D. (1998) *Proc. Natl. Acad. Sci. U.S.A. 95*, 8428−8430.
5. Uchida, Y., Takio, K., Titani, K., Ihara, Y., and Tomonaga, M. (1991) *Neuron 7*, 337−347.
6. Quaife, C. J., Findley, S. D., Erickson, J. C., Froelick, G. J., Kelly, E. J., Zambrowicz, B. P., and Palmiter, R. D. (1994) *Biochemistry 33*, 7250−7259.
7. Uchida, Y., Ihara, Y., and Tomonaga, M. (1988) *Biophys. Res. Commun. 150*, 1263−1267.
8. Uchida, Y., and Tomonaga, M. (1989) *Brain Res. 481*, 190−193.
9. Erickson, J. C., Sewell, A. K., Jensen, L. T., Winge, D. R., and Palmiter, R. D. (1994) *Brain Res. 649*, 297−304.
10. Kobayashi, H., Uchida, Y., Ihara, Y., Nakajima, K., Kohsaka, S., Miyatake, T., and Tsuji, S. (1993) *Brain Res. Mol. Brain Res. 19*, 188−194.
11. Palmiter, R. D., Findley, S. D., E., W. T., and Durnam, D. M. (1992) *Proc. Natl. Acad. Sci. U.S.A. 89*, 6333−6337.
12. Palmiter, R. D. (1995) *Toxicol. Appl. Pharmacol. 135*, 139−146.
13. Masters, B. A., Quaife, C. J., Erickson, J. C., Kelly, E. J., Froelick, G. J., Zambrowicz, B. P., Brinster, R. L., and Palmiter, R. D. (1994) *J. Neurosci. 14*, 5844−5857.
14. Erickson, J. C., Hollopeter, G., Thomas, S. A., Froelick, G. J., and Palmiter, R. D. (1997) *J. Neurosci. 17*, 1271−1281.
15. Arseniev, A., Schultze, P., Wörgötter, E., Braun, W., Wagner, G., Vašák, M., Kägi, J. H. R., and Wüthrich, K. (1988) *J. Mol. Biol. 201*, 637−657.
16. Schultze, P., Wörgötter, E., Braun, W., Wagner, G., Vašák, M., Kägi, J. H. R., and Wüthrich, K. (1988) *J. Mol. Biol. 203*, 251−268.
17. Messerle, B. A., Schäffer, A., Vašák, M., Kägi, J. H. R., and Wüthrich, K. (1990) *J. Mol. Biol. 214*, 765−779.

18. Robbins, A. H., McRee, D. E., Williamson, M., Collett, S. A., Xuong, N. H., Furey, W. F., Wang, B. C., and Stout, C. D. (1991) *J. Mol. Biol. 221*, 1269−1293.
19. Zangger, K., Öz, G., Otvos, J. D., and Armitage, I. M. (1999) *Protein Sci. 8*, 2630−2638.
20. Otvos, J. D., and Armitage, I. M. (1980) *Proc. Natl. Acad. Sci. U.S.A. 77*, 7094−7098.
21. Sewell, A. K., Jensen, L. T., Erickson, J. C., Palmiter, R. D., and Winge, D. R. (1995) *Biochemistry 34*, 4740−4747.
22. Bogumil, R., Faller, P., Pountney, D. L., and Vašák, M. (1996) *Eur. J. Biochem. 238*, 698−705.
23. Faller, P., and Vašák, M. (1997) *Biochemistry 36*, 13341−13348.
24. Hasler, D. W., Faller, P., and Vašák, M. (1998) *Biochemistry 37*, 14966−14973.
25. Faller, P., Hasler, D. W., Zerbe, O., Klauser, S., Winge, D. R., and Vašák, M. (1999) *Biochemistry 38*, 10158−10167.
26. Ellman, G. L. (1959) *Arch. Biochem. Biophys. 82*, 70−77.
27. Vašák, M. (1991) *Methods Enzymol. 205*, 452−458.
28. Okar, D. A., Felicia, N. D., Gui, L., and Lange, A. J. (1997) *Protein Expr. Purif. 11*, 79−85.
29. Kumar, A., Ernst, R. R., and Wüthrich, K. (1980) *Biochem. Biophys. Res. Commun. 95*, 1−6.
30. Braunschweiler, L., and Ernst, R. R. (1983) *J. Magn. Reson. 53*, 521−528.
31. States, D., Haberkorn, R., and Ruben, D. (1982) *J. Magn. Reson. 48*, 286−292.
32. Piotto, M., Saudek, V., and Sklenár, V. (1992) *J. Biomol. NMR 2*, 661−665.
33. Wishart, D. S., Bigam, C. G., Yao, J., Abildgaard, F., Dyson, H. J., Oldfield, E., Markley, J. L., and Sykes, B. D. (1995) *J. Biomol. NMR 6*, 135−140.
34. Shaka, A., Lee, C., and Pines, A. (1988) *J. Magn. Reson. 77*, 274−293.
35. Live, D., Armitage, I. M., Dalgarno, D. C., and Cowburn, D. (1985) *J. Am. Chem. Soc. 107*, 1775−1777.
36. Shaka, A. J., Keeler, J., and Freeman, R. (1983) *J. Magn. Reson. 53*, 313−340.
37. Farrow, N. A., Muhandiram, R., Singer, A. U., Pascal, S. M., Kay, C. M., Gish, G., Shoelson, S. E., Pawson, T., Forman-Kay, J. D., and Kay, L. E. (1994) *Biochemistry 33*, 5984−6003.
38. Johnson, B. A., and Blevins, R. A. (1994) *J. Biomol. NMR 4*, 603−614.
39. Clore, G. M., Driscoll, P. C., Wingfield, P. T., and Gronenborn, A. M. (1990) *Biochemistry 29*, 7387−73401.
40. Brünger, A. T., Clore, G. M., Gronenborn, A. M., and Karplus, M. (1986) *Proc. Natl. Acad. Sci. U.S.A. 83*, 3801−3805.
41. Nilges, M., Clore, G. M., and Gronenborn, A. M. (1988) *FEBS Lett. 229*, 317−324.
42. Laskowski, R. A., Rullmannn, J. A., MacArthur, M. W., Kaptein, R., and Thornton, J. M. (1996) *J. Biomol. NMR 8*, 477−486.
43. Šali, A., and Blundell, T. L. (1993) *J. Mol. Biol. 234*, 779−815.
44. Wüthrich, K. (1986) *NMR of Proteins and Nucleic Acids*, John Wiley & Sons, Inc., New York.
45. Pountney, D. L., Fundel, S. M., Faller, P., Birchler, N. E., Hunziker, P., and Vašák, M. (1994) *FEBS Lett. 345*, 193−197.
46. Kille, P., Hemmings, A., and Lunney, E. A. (1994) *Biochim. Biophys. Acta 1205*, 151−161.
47. Öz, G., Pountney, D. L., and Armitage, I. M. (1998) *Biochem. Cell. Biol. 76*, 223−234.
48. Mandel, A. M., Akke, M., and Palmer, A. G., 3rd. (1995) *J. Mol. Biol. 246*, 144−163.
49. Lipari, G., and Szabo, A. (1982) *J. Am. Chem. Soc. 104*, 4546−4559.
50. Lipari, G., and Szabo, A. (1982) *J. Am. Chem. Soc. 104*, 4559−4570.
51. Cornell, N. W., and Crivaro, K. E. (1972) *Anal. Biochem. 47*, 203−208.
52. Wagner, G., Neuhaus, D., Wörgötter, E., Vašák, M., Kägi, J. H. R., and Wüthrich, K. (1986) *J. Mol. Biol. 187*, 131−135.
53. Wright, P. E., and Dyson, H. J. (1999) *J. Mol. Biol. 293*, 321−331.
54. Fetrow, J. S., Siew, N., and Skolnick, J. (1999) *FASEB J. 13*, 1866−1874.
55. Hasler, D. W., Jensen, L. T., Zerbe, O., Winge, D. R., and Vašák, M. (2000) *Biochemistry 39*, 14567−14575.
56. Williamson, M. P. (1994) *Biochem. J. 297*, 249−260.
57. Riek, R., Prêcheur, B., Wang, Y., Mackay, E. A., Wider, G., Güntert, P., Liu, A., Kägi, J. H. R., and Wüthrich, K. (1999) *J. Mol. Biol. 291*, 417−428.
58. Daragan, V. A., and Mayo, K. H. (1997) *J. Prog. Nucl. Magn. Res. Spectrosc. 31*, 63−105.
59. Campos-Olivas, R., Newman, J. L., and Summers, M. F. (2000) *J. Mol. Biol. 296*, 633−649.
60. Garner, E., Cannon, P., Romero, P., Obradovic, Z., and Dunker, A. K. (1998) *Genome Inform. Ser. Workshop Genome Inform. 9*, 201−213.
61. Rogers, S., Wells, R., and Rechsteiner, M. (1986) *Science 234*, 364−368.
62. Rechsteiner, M., and Rogers, S. W. (1996) *Trends Biochem. Sci. 21*, 267−271.
63. URL for the sequence analysis program: http://www.at.embnet.org/embnet/tools/bio/PESTfind/
64. McKim, J. M., Jr., Choudhuri, S., and Klaassen, C. D. (1992) *Toxicol Appl Pharmacol 116*, 117−24.
65. Karin, M., Haslinger, A., Heguy, A., Dietlin, T., and Imbra, R. (1987) *EXS 52*, 401−405.
66. Gedamu, L., Varshney, U., Jahroudi, N., Foster, R., and Shworak, N. W. (1987) *EXS 52*, 361−372.
67. Koradi, R., Billeter, M., and Wüthrich, K. (1996) *J. Mol. Graph. 14*, 51−55, 29−32.

BI010827L